

SHIFTS: Simulator for the Herschel Imaging Fourier Transform Spectrometer

John V. Lindner^{*a}, David A. Naylor^a, Bruce M. Swinyard^b,

^aDepartment of Physics, University of Lethbridge, Lethbridge, Alberta, Canada.

^bRutherford Appleton Laboratory, Chilton, Oxfordshire, England.

ABSTRACT

The Spectral and Photometric Imaging Receiver (SPIRE) is one of three scientific instruments on the European Space Agency's (ESA) Herschel Space Observatory (HSO). The medium resolution spectroscopic capabilities of SPIRE are provided by an imaging Fourier transform spectrometer (IFTS). A software simulator of the SPIRE IFTS was written to create realistic data products, making use of available qualification and test data. A graphical user interface (GUI) provides fast and flexible access to the simulation engine. We present the design and integration of the simulator, as well as results from the simulator predicting the instrument performance under varying operational conditions.

Keywords: Herschel, SPIRE, Imaging Fourier Transform Spectrometer, Software Simulation

1. INTRODUCTION

The Herschel Space Observatory (HSO) is a cornerstone mission of the European Space Agency (ESA). With a 3.5 m passively cooled primary mirror, cryogenically cooled instrument payload and an orbit at the second Lagrangian point (L2), Herschel will provide unparalleled sensitivity between 60 and 670 μm . Scheduled for launch in 2008, the scientific payload of the HSO consists of three onboard instruments: the Heterodyne Instrument for the Far Infrared (HIFI), the Photodetector Array Camera and Spectrometer (PACS), and the Spectral and Photometric Imaging Receiver (SPIRE).^{1,2}

The primary scientific goals of the SPIRE instrument are characterizing the spectral energy distributions of redshifted galaxies and studying interstellar gas and dust before and during star formation. To accomplish these goals, SPIRE contains two sub-instruments: an imaging photometer and an imaging Fourier transform spectrometer (IFTS).¹

As with most space missions, post-launch repairs are impractical and thus, a comprehensive instrument test campaign is necessary. The first and second proto-flight model (PFM1 and PFM2, respectively) test campaigns were conducted at the Rutherford Appleton Laboratory (RAL) in Oxfordshire, England in 2005.^{3,4} The final instrument test campaigns are planned for Spring/Summer 2006 with delivery of the SPIRE flight model to ESA scheduled for August 2006.

Concurrent to the instrument test campaigns, software simulators of the two SPIRE sub-instruments were written.^{1,5,6} This paper describes the design, implementation and integration of the Simulator for the Herschel Imaging Fourier Transform Spectrometer (SHIFTS). Based on a simple conceptual model developed by Dr Bruce Swinyard at RAL, SHIFTS generates realistic data products for the SPIRE imaging spectrometer using existing subsystem qualification data.^{5,7} Three primary goals motivated this work: First, the SPIRE software teams can evaluate their data reduction programs using the data products generated by SHIFTS.¹ Second, SPIRE instrument teams and the astronomical community can use SHIFTS to predict instrument performance under various operating conditions and plan their observing proposals accordingly. Finally, SHIFTS can assist in the characterization and diagnosis of problems encountered during both ground testing and in flight.

This paper contains five sections: Section 2 describes the various components of the SPIRE spectrometer. Section 3 outlines the design and implementation of SHIFTS. Section 4 compares SHIFTS-simulated data to results measured during the PFM1 test campaign. Section 5 provides conclusions and suggestions for future directions.

*E-mail: john.lindner@uleth.ca; Telephone: (403) 329-2719; Fax: (403) 329-2057; www.uleth.ca/phy/naylor/

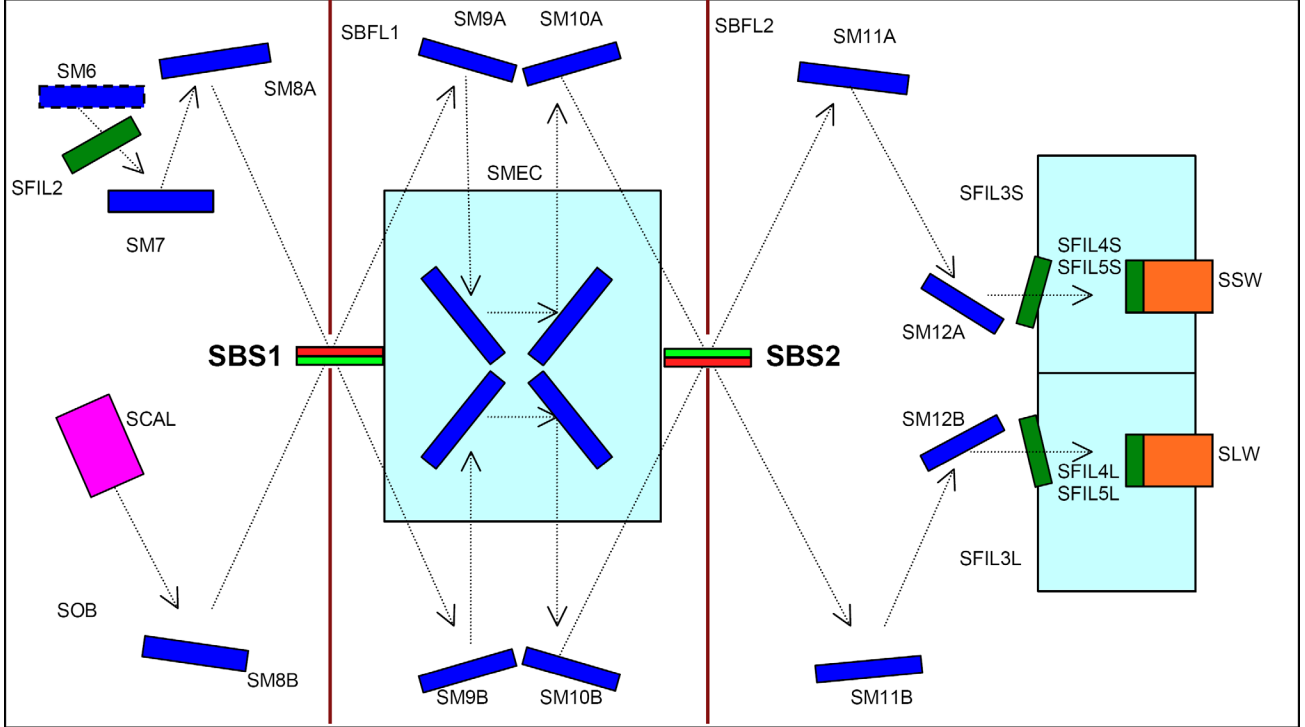


Figure 1. Schematic of the SPIRE spectrometer. The dotted arrows denote the direction light travels; the dark blue boxes denote mirrors; the dark green boxes denote filters; the light blue boxes denote the spectrometer mechanism and the 1.7 K enclosure (from left to right); the orange boxes denote the bolometer detector assemblies; the pink box denotes the spectrometer calibrator; and the red/green boxes denote the beamsplitters (red corresponds to the inductive side and green to the capacitive side of the beamsplitter). The SM6 mirror is dashed to indicate its location on the photometer side of the focal plane unit. (Figure courtesy of Dr Douglas Griffin, Rutherford Appleton Laboratory, Oxfordshire, England.)

2. THE SPIRE SPECTROMETER

This section describes the optical layout of the SPIRE spectrometer. Figure 1 shows a schematic of the spectrometer side of the SPIRE focal plane unit (FPU). Note the symmetry of the spectrometer about an imaginary line between the two beamsplitters; this figure shows the position of zero path difference (ZPD). The FPU must be cooled to below at least 4.5 K by the Herschel cryostat because the peak blackbody emission of any surface between 7 and 25 K falls within the SPIRE band.

The SPIRE spectrometer is of the *Mach-Zehnder* (MZ) design.⁸ The MZ design provides access to the two input and two output ports of the interferometer. In the SPIRE design, the arms of the classic MZ interferometer are folded to reduce both the mass and volume of the interferometer (critical parameters for any space mission). This folding allows a single translation stage to simultaneously vary the optical path of both beams. Therefore, a change of Δx in stage position changes the optical path difference (OPD) between the two beams by $4\Delta x$.⁸

At the entrance to the spectrometer, the telescope beam passes through a low-pass filter (SFIL2 in Figure 1) and is folded by several mirrors (SM7 and SM8A) onto the first *beamsplitter*.¹ Incident on the opposite face of the beamsplitter is light from the *spectrometer calibrator* (SCAL) source, which compensates for the large background emission of the Herschel primary and secondary mirrors.⁹ The reflected and transmitted beams are directed to complementary collimating mirrors (SM9A and SM9B) that fold the beams onto the back-to-back roof-top mirrors mounted on the *spectrometer mechanism* (SMEC), which provides the optical retardation for the interferometer. Following reflection from the roof-top mirrors, the beams are folded back to the camera mirrors (SM10A and SM10B) and then directed to the second beamsplitter (SBS2).¹ Finally, two pairs of mirrors direct the beams through separate low-pass filters (SFIL3S and SFIL3L) into the 1.7 K enclosure of the bolometer detector assemblies (BDAs), which house the detection systems for the two spectrometer bands.^{1,5}

Table 1. Description of SHIFTS modules.

Module	Description
SMECMPD	Simulated the mechanical path difference of the spectrometer mechanism given a noise profile (see Section 3.1).
THERMALHPM	Calculated the temperature of the Herschel primary mirror given a drift rate (see Section 3.2).
THERMALSCAL	Simulated the temperature of the two spectrometer calibrator sources given a noise profile (see Section 3.3).
POINTINGHSO	Calculated the pointing of the Herschel telescope given absolute and relative pointing errors (see Section 3.4).
POWERBOLO	Simulated the modified Mach-Zehnder interferometer by calculating the power incident on each bolometer given a simulated astronomical source and the above four timelines (see Section 3.5).
DETECTORSIG	Calculated the signal measured by the bolometer and read out by the electronics given the power incident on each bolometer (see Section 3.6).

The detector arrays consist of 19 and 37 pixels for the long and short wavelength bands (SLW and SSW), respectively. Inside the BDAs, each beam passes through a *low-pass filter stack* and is focused onto the *feedhorns*. The feedhorns act as high-pass filters and couple the light to the *spider-web bolometers*. Cooled to 300 mK by an internal Helium-3 refrigerator, the bolometers detect the incident radiation. The measured signal is then filtered, digitized and read out by the detector electronics.¹

3. THE SPIRE SPECTROMETER SIMULATOR

This section describes the design and implementation of SHIFTS. SHIFTS was written to model the components and subsystems of the SPIRE spectrometer outlined in Section 2. The elements included represent the subsystems that have the greatest effect on the measured interferogram. One potential source of noise not included in SHIFTS is the pointing errors of the beam steering mirror; there was insufficient test data available at the time of publication to characterize its effect.

The simulator is written in the Interactive Data Language (IDL[®]), which is well-suited to a project such as SHIFTS because of its powerful array manipulation capabilities and extensive visualization tools. Some of the software architecture of SHIFTS is based on the structure of the SPIRE photometer simulator.⁶ SHIFTS is composed of a series of self-contained modules, each simulating a physical quantity of the SPIRE spectrometer. In common with the SPIRE photometer simulator, the output of each module is a single timeline representing the physical quantity being simulated (e.g., the position of the spectrometer mechanism). Table 1 lists and describes the primary modules in SHIFTS.

A master control program (MCP) controls the interaction between the modules, retrieving the module-generated timelines representing different modelled parameters. The modular nature of SHIFTS allows the most current characterization of a specific subsystem to be easily integrated without affecting the rest of the simulator.

The MCP is controlled by an IDL graphical user interface (GUI). Figure 2 shows a screen capture of the SHIFTS GUI in the expert user mode. In this mode, an extensive set of parameters are available, allowing the user to control every element of the simulation. A second, common user, mode provides the same level of access as the actual instrument so astronomers can explore the capabilities of the SPIRE spectrometer without having to understand the detailed operation of the instrument.

When SHIFTS is first executed, an initialization routine populates the data structures by reading into memory various calibration files, as well as the simulated astronomical source (SAS). With reference to a master time

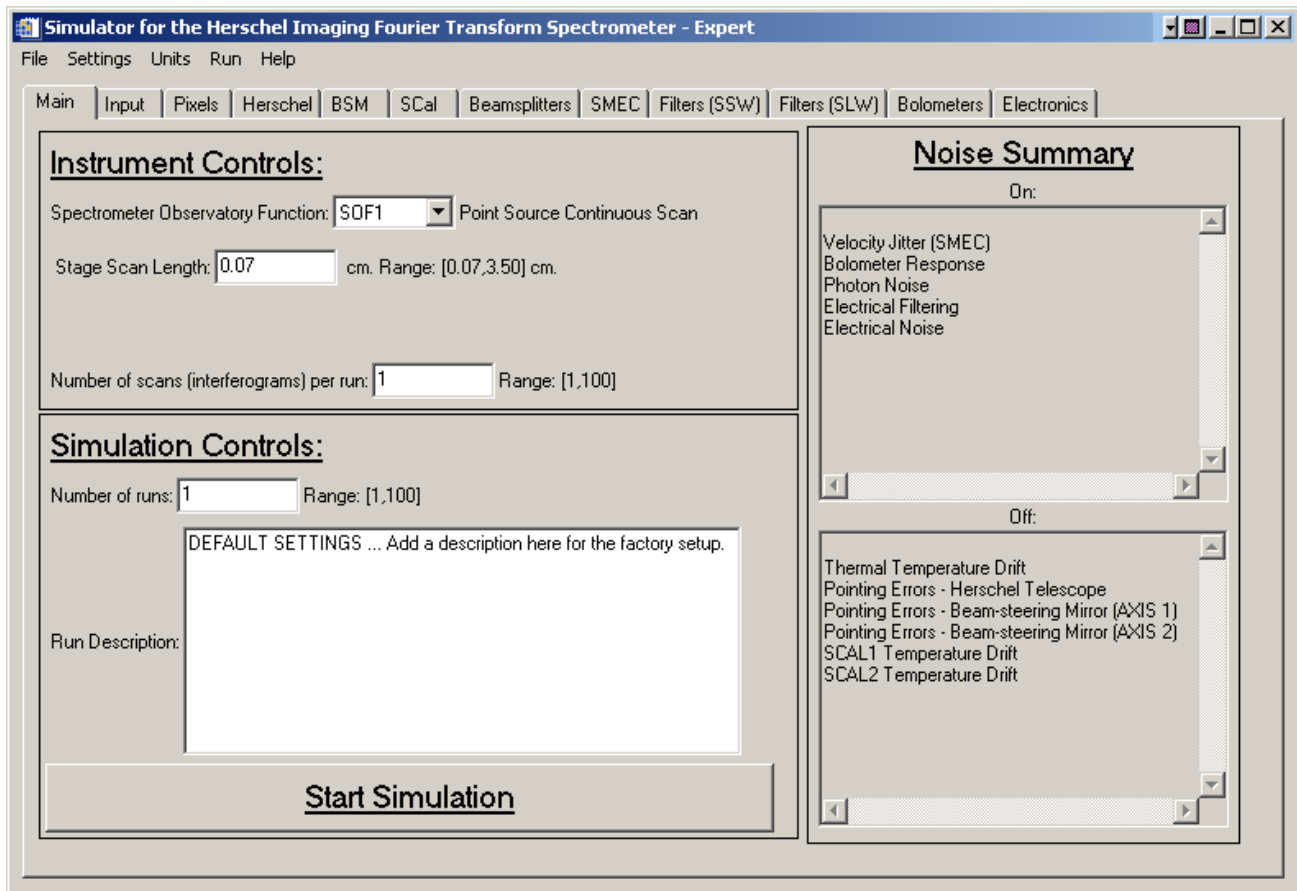


Figure 2. Screen capture of the SHIFTS graphical user interface in the expert user mode. The text boxes on the right summarize the elements included in the simulation; each tab controls a separate aspect of the simulator.

grid, the independent timelines for the stage position, the pointing of the Herschel telescope, and the temperature of the primary mirror and SCAL sources are all simulated in parallel. A radiative transfer model simulates the propagation of radiation through the SPIRE spectrometer to determine the power incident on the bolometer. Finally, the measured signal is sampled onto a Herschel data product timeline. A single high resolution scan requires approximately ten minutes to generate on a 2.52 GHz computer with 1 gigabyte of RAM.

The astronomical input to SHIFTS is a simulated source, a time-independent three-dimensional (two spatial and one spectral) data cube where each element of the cube is a specific intensity given in janskies per steradian. The SAS data cube is converted from a specific intensity to an electrical field per unit wavenumber. This conversion assumes a single-mode throughput of $A\Omega = \lambda^2$ given the geometric area of the entrance aperture (i.e., the Herschel primary mirror) in a diffraction-limited case.¹ However, it became evident during the test campaigns that this approximation was not strictly valid.^{3,4} Since we currently lack the data required to determine the wavelength dependence of the beam, the above assumption was used in our analysis.

As indicated above, the six timelines generated by SHIFTS (see Table 1) are referenced to the same master time grid, corresponding to a 500 Hz error-free clock. Since the highest frequency component modelled in SHIFTS is 113.06 Hz, the master time grid represents an oversampling of slightly more than two. The following sections describe the key features of the six modules listed in Table 1.

3.1. Position of the spectrometer mechanism

As indicated above, the optical path difference of the interferometer is varied by the spectrometer mechanism (SMEC).¹ SMEC consists of back-to-back roof-top mirrors mounted on a translation stage.^{1,7} The variable

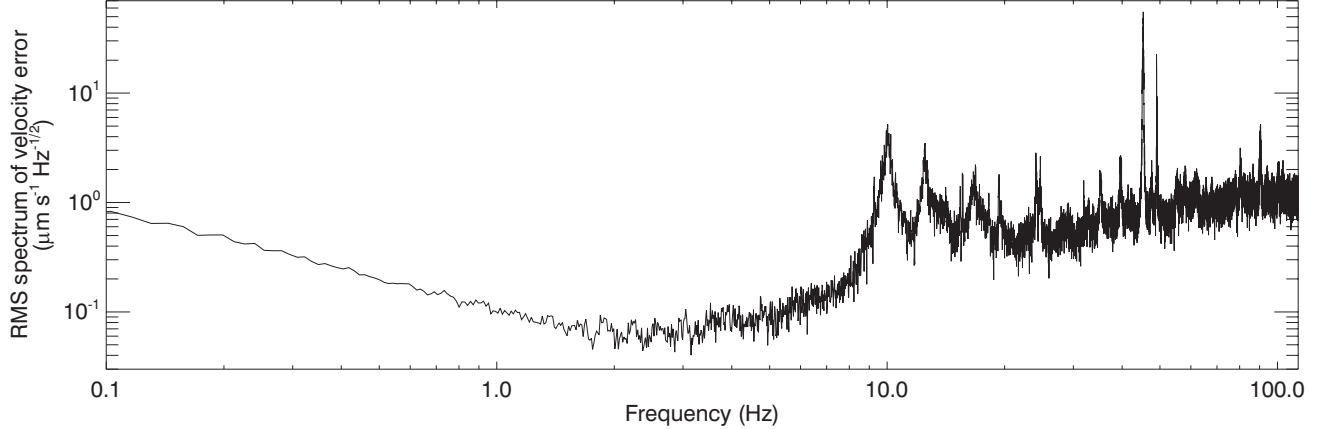


Figure 3. Model profile of velocity error from the spectrometer mechanism. The profile was determined from the velocity error spectra of 8 scans taken at $452 \mu\text{m s}^{-1}$ during the PFM1 test campaign.

scan length produces spectral resolutions up to 0.047 cm^{-1} . This section outlines the SMECMPD module that simulates the mechanical path difference (MPD) of SMEC.

SMEC operates in a continuous scan mode at a constant velocity controlled by a digital feedback loop.¹ In reality, a constant velocity is unattainable. Since variations in the SMEC velocity are equivalent to variations in the frequency components of the modulated infrared radiation, it is important to characterize the effect of the SMEC stage on the retrieved spectrum.¹⁰ To investigate this problem, the SMECMPD module utilizes SMEC measurements from the PFM1 tests.⁴ The resulting noise profile, shown in Figure 3, was determined from the metrology of 8 scans taken at a mean stage speed of $452 \mu\text{m s}^{-1}$. To generate realistic stage positions, the above noise profile is first interpolated onto the master time grid. Uniform random phase between $-\pi$ and π radians is then added to each point in the profile. A simulated velocity error, Δv_m , is determined by computing the Fourier transform of the randomized profile. Finally, the mechanical path difference at each master time interval m is calculated by

$$z_m = v_m \Delta t_m + z_{m-1} - z_o, \quad [\text{cm}] \quad (1)$$

where z_o is the initial position of the scan (in cm), Δt_m is the master time spacing (in s) and $v_m = \bar{v} + \Delta v_m$ is the sum of the user-defined stage velocity and the simulated velocity error (in cm s^{-1}).

A single run of SHIFTS consists of one or more scans, each producing its own interferogram. Even though each scan is based on the same velocity noise distribution (see Figure 3), they all differ from each other due to the random nature of the phase introduced.

3.2. Temperature of the Herschel primary mirror

The HSO has a 3.5 m diameter passively cooled primary mirror.^{1,2} The primary and secondary mirrors will emit radiation as blackbodies with temperatures between 70 and 90 K and emissivities between 1 and 3%.¹ The exact temperature and emissivity of the mirrors cannot be determined until the HSO is in orbit because the thermal conditions of the spacecraft at L2 are largely unknown.⁹ However, their temperatures are expected to be relatively constant because of their large thermal masses and stable environment. The THERMALHPM module simulates the temperature of the mirror as a simple linear drift, characterized by a drift rate of 180 mK hr^{-1} and an initial temperature of 80 K.^{1,5,11}

3.3. Temperature of the spectrometer calibrator

Emission from the primary and secondary mirrors will be the dominant source of noise in the SPIRE spectrometer.¹ To minimize the dynamic range of the modulated signal of the interferometer, the second input port of the SPIRE spectrometer is illuminated by the spectrometer calibrator (SCAL; see Figure 1), a continuum source with similar spectral characteristics as the background signal from the telescope.

SCAL employs two sources, SCAL-A and SCAL-B, each consisting of an Aluminum end cap mounted on a Torlon strut. While only these two sources are heated, the entire mechanism is painted with a high-emissivity coating.⁹ Since SCAL is located at a pupil (and is therefore seen equally by all pixels), the geometric area of the sources defines their effective emissivity. Therefore, the two sources produce effective emissivities of 2 and 4% defined by their geometry. The operating range of the SCAL sources is 4–120 K.^{1,9}

The temperatures of the SCAL sources are controlled by a similar feedback loop as SMEC. We determined a noise profile (not shown) for the SCAL sources based on temperature measurements from the PFM1 tests.⁵ Repeating the technique outlined in Section 3.1, a randomized temperature error, ΔT_m (in K), is determined. The temperature at each master time interval m is then given by

$$T_m = \bar{T} + \Delta T_m, \quad [\text{K}] \quad (2)$$

where \bar{T} is the user-defined temperature of the source. This technique is employed for both SCAL sources.

3.4. Pointing of the Herschel telescope

The large inertial mass of Herschel will ensure the pointing is relatively stable and not subject to high-frequency variations. The orientation of the HSO determines the FOV seen by the detectors.¹ Two pointing errors are included in SHIFTS: the absolute pointing error (APE) and the relative pointing error (RPE). The APE is defined as an initial offset with a one standard deviation error of 1.2 arcsec per axis while the RPE is defined as a drift over 60s with a one standard deviation error of 0.3 arcsec per axis.¹¹ The magnitude of the RPE and APE are determined using Gaussian noise. The randomized APE and RPE values specify the intercept and slope, respectively, of both the right ascension and declination of the HSO.

3.5. Power incident on bolometers

This section describes the POWERBOLO module, the most complex module in SHIFTS. This module takes the four timelines described above and simulates the entire optical system of the SPIRE spectrometer to determine the power incident on a particular bolometer at each master time interval m . The POWERBOLO module produced 56 timelines, one for each bolometer (see Section 2).¹ The first four parts of Section 3.5 describe the calculations performed to determine the power incident on each bolometer f . The time-dependent nature of these values make it impossible to employ a simple inverse Fourier transform on the SAS spectra. Instead, the power is calculated one master time interval at a time, beginning at $m = 0$. The addition of photon noise is described in Section 3.5.5.

3.5.1. Determining the sky section viewed by each feedhorn

Before the radiation from the SAS is propagated through the optical system, the spatial pixels of the simulated astronomical source are first grouped into their respective feedhorns. The point spread function of the SPIRE detectors is still under investigation so its coupling to the Herschel telescope was simplified in SHIFTS. The FOV of the SPIRE spectrometer is 2.6 arcmin across; the angular spacing between the hexagonally packed SLW and SSW feedhorns is 49.0 and 28.3 arcsec, respectively.¹ An algorithm was written to determine the current FOV of each detector feedhorn f . The angular distance between the spatial position of each SAS pixel ij and the center of each feedhorn f is iteratively calculated by

$$r_{ijf} = \sqrt{(\alpha_f - \alpha_{im})^2 + (\delta_f - \delta_{jm})^2}, \quad [\text{arcsec}] \quad (3)$$

where α_f and δ_f are the angular positions of the center of feedhorn f (relative to the central feedhorn), α_{im} and δ_{jm} are the right ascension and declination, respectively, of the SAS pixel ij at time interval m (all in arcsec). The calculation of the values α_{im} and δ_{jm} is described in Section 3.4. If the distance r_{ijf} is less than the angular radius of the feedhorn, then the spectrum of SAS pixel ij is considered inside feedhorn f . Once SHIFTS determined which SAS pixels enter each feedhorn, their respective spectra are summed.

3.5.2. Modelling the background emission

The largest noise source in the SPIRE spectrometer is the blackbody emission from the Herschel primary mirror and SCAL.^{1,9} Since the temperatures of the Herschel primary mirror and the SCAL sources change over time, the corresponding changes in their blackbody emission have to be calculated. The thermal emission from other components in the SPIRE spectrometer are not included in SHIFTS. In the radiative transfer model, the specific intensities of all thermal sources are converted to electric fields per unit wavenumber.

In the case of the emission from the Herschel telescope, the secondary mirror is included as an additional contribution to the emissivity of the primary mirror. The total emissivity of the mirrors is therefore assumed to be a constant 4% (2% from each mirror) over the SPIRE wavelength range.^{1,9} The blackbody emission of the Herschel telescope is then calculated given the temperature timeline described in Section 3.2.

As for the emission from the calibration port, the temperature timelines of the two heated sources, SCAL-A and SCAL-B, were described in Section 3.3. The current release of SHIFTS ignores the minor wavelength dependence of the black coating and assumes that both sources are perfect emitters.⁹ The same assumption is made for the third component of the SCAL emission, the remaining 94% of the pupil. The temperature of this contribution is fixed at 4.5 K (i.e., the temperature of the SPIRE FPU).^{1,9} The blackbody radiation from each component is summed to produce the total emission of SCAL.

3.5.3. Optical retardation and signal attenuation

From the calculations in the previous two sections, each radiation source (the SAS, the Herschel telescope and SCAL) yields two pairs of spectral beams for each bolometer. One pair is detected by the SLW bolometers while the other is detected by the SSW bolometers. Each pair represents the two optical paths between source and detector. Since the beams originate from different sources, they are incoherent and can be treated independently.

To simulate the optical retardation of each beam, we examine the optical path taken by an electromagnetic wave of amplitude E_k entering the first input port (i.e., the sky port) of the SPIRE spectrometer. For this discussion, we assume the back-to-back rooftop mirrors shown in Figure 1 are located a distance z below ZPD. The electric field is split into two separate beams at the first beamsplitter (SBS1 in Figure 1). The *up beam* is reflected off SBS1 while the *down beam* passes through SBS1. The up beam travels a longer optical distance between the two beamsplitters so its phase lags by a factor of $e^{-i4\pi\sigma z}$ relative to ZPD, where σ is the wavenumber (in cm^{-1}). Complementing the up beam, the phase of the down beam leads by a factor of $e^{i4\pi\sigma z}$ relative to ZPD. Upon recombination at the second beamsplitter, the optical path difference between the two beams is $4z$.⁸

For the beam directed to the SSW bolometers, the up beam is reflected off the second beamsplitter (SBS2) while the down beam is transmitted through SBS2. This results in an electric field per wavenumber incident on the SSW bolometer f_s at a master time interval m given by

$$E_{f_s m k} = E_{f_s m k} (r_1 r_2 e^{i4\pi\sigma_k z_m} + t_1 t_2 e^{-i4\pi\sigma_k z_m}), \quad [\text{V m}^{-1} (\text{cm}^{-1})^{-1}] \quad (4)$$

where r and t are the complex amplitude reflection and transmission coefficients, respectively, σ_k is the wavenumber (in cm^{-1}) and z_m is the stage position given by Equation 1. The subscripts on r and t denote the beamsplitter (SBS1 or SBS2). Similarly, the electric field of wavenumber k incident on the SLW bolometer f_ℓ at a master time interval m is given by

$$E_{f_\ell m k} = E_{f_\ell m k} (r_1 t_2 e^{i4\pi\sigma_k z_m} + t_1 r_2 e^{-i4\pi\sigma_k z_m}). \quad [\text{V m}^{-1} (\text{cm}^{-1})^{-1}] \quad (5)$$

The magnitudes of r and t are taken from measured values determined by the Astronomical Instrumentation Group (AIG) at Cardiff University.^{1,9} Equations 4 and 5 are used to simulate the optical retardation of the astronomical signal and the blackbody emission of the Herschel telescope. A complementary set of equations holds for radiation entering the SCAL input port.

In addition to the optical properties of the beamsplitter and the optical retardation introduced by SMEC, the other efficiencies of the optical system are also modelled in SHIFTS. These include the reflectance of the SPIRE mirrors, the low-pass filters and the various efficiencies of the detection system (i.e., aperture, feedhorn, main beam and spillover).¹ These efficiencies are combined into a single frequency-dependent amplitude transmission

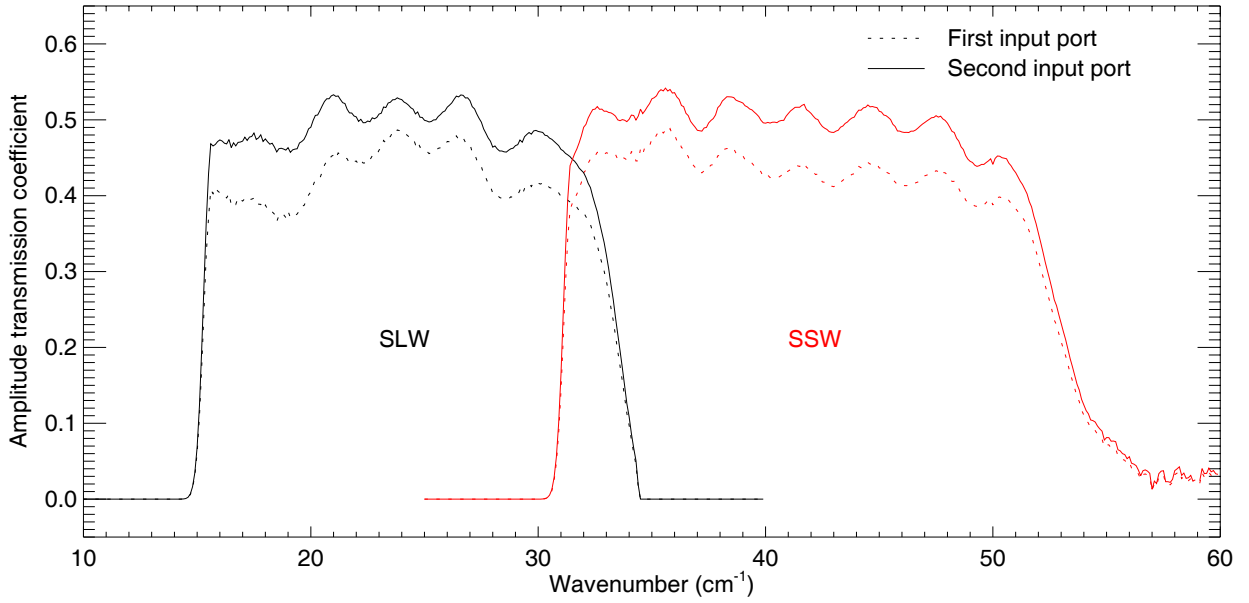


Figure 4. Transmission efficiency for the input and output ports of the SPIRE spectrometer. These profiles include effects of the beamsplitters; the low-pass filters; the mirrors; and the feedhorn, aperture, main beam and spillover efficiencies of the detection system.

coefficient given by η_k . We determined η_k for each input port-output port pair based on broadband qualification data and monochromatic simulations¹. The four efficiencies, which assume a single-mode propagation (i.e., TE₁₁), are shown in Figure 4. As expected, the transmission is higher for the SCAL port because there are fewer optical components (filters and mirrors) in its path.^{1,9} The product of each η_k and their respective electric fields (given by either Equation 4 or 5) yield the electric field of wavenumber k incident on each bolometer f at a master time interval m .

3.5.4. Integrating the power

Finally, after accounting for the various optical paths of the SPIRE spectrometer, the total power incident on bolometer f at a master time interval m is given by

$$I_{fm} = \Delta\sigma \sum_{\sigma_o}^{\sigma_N} \left(\frac{2A_f}{c\epsilon_o} E_{fmk}^* E_{fmk} \right), \quad [\text{W}] \quad (6)$$

where E_{fmk} is the electric field at a wavenumber k incident on bolometer f at a master time interval m (in $\text{V m}^{-1} (\text{cm}^{-1})^{-1}$); $\Delta\sigma$ is the line width of the SAS spectrum (in cm^{-1}); σ_o and σ_N are the lower and upper bounds, respectively, of the wavenumber grid (both in cm^{-1}); A_f is the area of the circular aperture of feedhorn f (in m^2); c is the speed of light and ϵ_o is the permittivity of free space.

Equation 6 represents the final step at each time step of the iteration process introduced at the beginning of Section 3.5. Following the summation, the master time interval is incremented to $m + 1$. At this new master time interval, the MPD of the SMEC stage, the temperature of SCAL and the Herschel primary mirror, and the pointing of the HSO are all different. The calculations of Sections 3.5.1 to 3.5.4 are repeated and the master time interval is then incremented again. This iterative process continues until the power incident on each bolometer is calculated for every master time interval. The result of these iterations is effectively a discrete Fourier transform (DFT) of the electromagnetic waves entering the two input ports.

3.5.5. Photon noise

Once a simulated interferogram was determined for each bolometer, the photon noise is calculated from the power. Proportional to the square root of the number of photons, the photon noise is generally given as a

noise-equivalent power (NEP).¹ In SHIFTS, the power of the photon noise is estimated by

$$\Delta I_{fm} = \sqrt{\left(\frac{2hc\sigma_o}{\Delta t_m}\right) I_{fm}}, \quad [\text{W}] \quad (7)$$

where h is the Planck constant, c is the speed of light, σ_o is the center wavenumber of each band (in cm^{-1}), Δt_m is the master time interval (in s) and I_{fm} is the power incident on bolometer f at a master time interval m (in W). For the SLW and SSW arrays, σ_o is set to 22.2 and 40 cm^{-1} (450 and 250 μm), respectively. Each value of ΔI_{fm} is multiplied by random Gaussian noise to simulate the random arrival time of photons. This simulated photon noise is added to the interferogram, I_{fm} , determined in the previous section.

3.6. Measured signal

From the results of Section 3.5, SHIFTS determines the power incident on each bolometer at every instance of the master time grid. The DETECTOR SIG module determines the actual signal measured by the SPIRE detection system.

Spider-web bolometers, located in an integrating cavity below the circular waveguide attached the base of the feedhorns, are used to detect the incident radiation.¹ By definition, a bolometer measures radiation by measuring changes in resistance generated by the absorbed radiation.¹² This change is not instantaneous but occurs with a characteristic time constant. The thermal response of the bolometer is simulated as a simple RC circuit. In addition to the thermal response of the bolometer, a seven-pole Bessel filter in the warm electronics of the Herschel service module has a characteristic response. The combination of the thermal and electrical responses yields the *impulse response function* (IRF). The response of the detection system is equivalent to a low-pass spectral filter.⁵ The IRF is convolved with the time-varying flux incident on each bolometer to simulate the response of the detection system as SMEC scans.⁵

Following the convolution of the IRF, each element in the interferogram is converted to a voltage by multiplying by the quantum efficiency (0.7) and the responsivity (40 GVW^{-1}) of the bolometers.^{1,11} The final step is the inclusion of electrical noise of the electrical amplifiers (5 $\text{nVHz}^{-1/2}$) using the method described in Section 3.5.5.

3.7. Readout

The last step in SHIFTS is the production of a synthetic data product defined by the detector voltages and the stage positions. While equal time sampling is necessary in SHIFTS, it does not reflect the actual sampling of the SPIRE spectrometer. To simplify the electronics, the stage metrology and the detector signal are sampled asynchronously at 226.12 and 80 Hz.¹ To mimic this sampling, SHIFTS shifts the signal and position onto their proper grids using a cubic spline interpolation. However, in contrast to the actual signal measurements, the SHIFTS detector signal was not then digitized.

Once the position and signal were interpolated onto their respective time grids, the results were saved to an external electronic file. Telemetry data from the HSO will be accessible as a file in FITS format.¹³ Similarly, SHIFTS saves the stage metrology and detector signal timelines to FITS files containing the same data and metadata as the Herschel FITS files.

4. RESULTS AND DISCUSSION

This section compares a real and synthetic SPIRE data product. The synthetic data was generated by SHIFTS while the real instrument data was collected during the PFM1 test campaign conducted at RAL in 2005. Results from the PFM1 test campaign are detailed in Lim *et al.*,⁴ Naylor *et al.*¹⁴ and Spencer, Naylor & Swinyard.¹⁵

In brief, the PFM1 version of SPIRE was mounted inside a test cryostat to simulate the spacecraft thermal environment that will be experienced at L2. The sky port of the SPIRE spectrometer viewed the test facility through the cryostat window or, by insertion of a flip mirror, an internal cryogenic blackbody (CBB) source. Manufactured in a similar fashion to SCAL, the CBB was a blackened source that filled the FOV and was used to mimic the thermal emission of the Herschel primary mirror.⁴

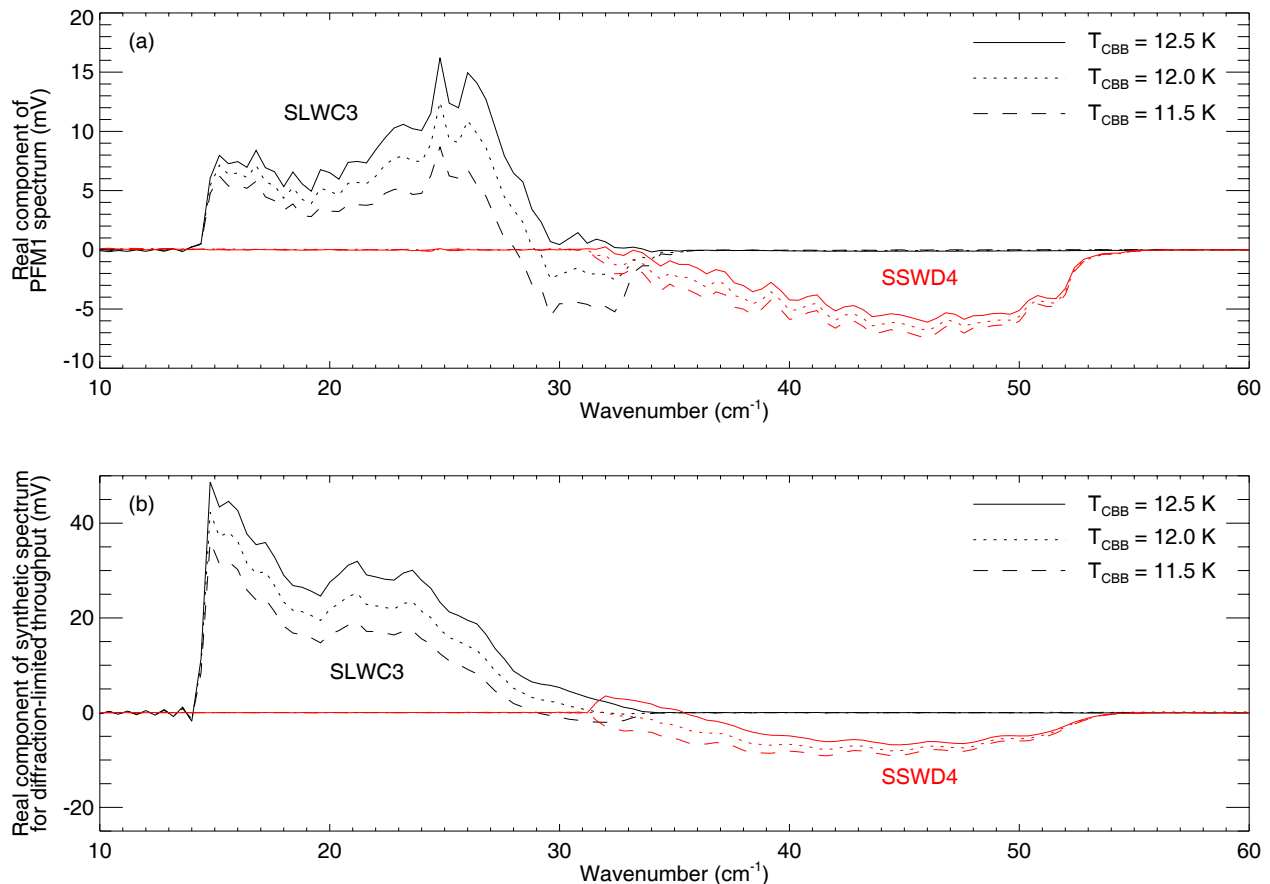


Figure 5. Compensation of real and synthetic spectra. Panel (a) shows the real spectra for the three cryogenic blackbody temperatures; Panel (b) represents the synthetic spectra generated by SHIFTS.

The data set under analysis was measured on March 24, 2005 when the CBB and the two SCAL sources were heated. As previously indicated, accurate compensation of the Herschel primary mirror is an extremely important component of calibration in the SPIRE spectrometer. This comparison investigated 3 sets of 10 medium resolution scans ($\Delta\sigma = 0.47 \text{ cm}^{-1}$) of the central pixels in each array (SLWC3 and SSWD4) taken at a stage speed of $302 \mu\text{m s}^{-1}$. The SCAL-A and SCAL-B sources were fixed at 38 and 6 K, respectively, for the duration of these scans. The CBB temperature was incremented, in steps of 0.5 K, from 11.5 to 12.5 K.

To simulate the March 24 data, SHIFTS was executed under the conditions outlined above. The stage velocity jitter and the electrical and photon noise were included, as were the bolometer and electrical responses (see Sections 3.1, 3.5.5 and 3.6). The SLWC3 and SSWD4 thermal time constants (i.e., the central pixels in each array) were set to 12.40 and 5.97 ms.¹⁶

To reduce the data, the data-processing pipeline for the SPIRE spectrometer was employed.¹⁷ The input to the pipeline are the data products described in Section 3.7. The pipeline accepts both real (e.g., PFM1) and SHIFTS-simulated data products. In the case of real data, the detectors signals were given in analog-to-digital units (ADUs). A 16-bit analog-to-digital converter (ADC) in the SPIRE warm electronics digitizes voltages between 0 and 5 V.⁵ To allow absolute power comparisons, we converted all the real detector signals from ADUs to voltages using a fixed scaling factor.

Figure 5 compares the real and synthetic PFM1 spectra for both arrays. Panel (a) shows the real spectra determined from double-sided interferograms. Negative spectra indicate that the SCAL port was dominant.

For CBB temperatures of 11.5 and 12.0 K, the dominance of the ports in the real SLWC3 spectra switched at approximately 28 and 29 cm^{-1} , respectively.

Panel (b) shows the synthetic spectra generated by SHIFTS. The synthetic spectra reproduce the basic features of the real spectra: a net positive spectra was seen for low frequencies and a net negative spectra was seen for high frequencies. Furthermore, the synthetic SLWC3 spectrum for a CBB temperature of 11.5 K became dominated by the SCAL port at approximately 28 cm^{-1} , in agreement with the real spectrum.

However, there were distinct differences between the spectra. Examining the distribution of energy within each band, it was clear that the synthetic spectra in Panel (b) contained more energy at low wavenumbers than was seen in the real data in Panel (a). One potential explanation for this result was the failure of the single mode approximation mentioned in Section 3. Since the broadband wavelength-dependent weighting of the radiation modes is currently unknown, we assumed all radiation propagated in the fundamental mode (i.e., TE_{11}). However, Griffin¹⁸ suggests that at least 30% of the radiation absorbed by the bolometers will be contained in higher order modes. Only present at higher frequencies, the higher order modes would tend to flatten out the SHIFTS spectra, as was seen in the real data. Unfortunately, modelling the power in the other modes is currently beyond the scope of SHIFTS. However, this section demonstrated that SHIFTS well represents the spectral behaviour of the compensation scheme.

5. CONCLUSION

This paper presented the design and implementation of the Simulator for the Herschel Imaging Fourier Transform Spectrometer.^{1,5} SHIFTS was written to simulate the performance of the Spectral and Photometric Imaging Receiver spectrometer, an imaging Fourier transform spectrometer mounted onboard the Herschel Space Observatory.²

SHIFTS has already proved helpful in debugging the spectrometer data-processing pipeline under construction at the University of Lethbridge. The simulator is also being employed in the data analysis of existing and future SPIRE instrument test results. SHIFTS is being released to the SPIRE consortium at the time of publication; a wider release is planned for Fall 2006, to coincide with the initial call for Herschel observing proposals.

ACKNOWLEDGMENTS

JVL is indebted to the AIG at the University of Lethbridge for their help. Special thanks go to Peter Davis, Trevor Fulton, Ian Schofield, Troy Ronda and Locke Spencer. In addition to the AIG at the University of Lethbridge, JVL would like to thank other members of the SPIRE consortium for their assistance: Professor Peter Ade (Cardiff University, Cardiff, Wales), Dr Jean-Paul Baluteau (Laboratoire d'Astrophysique de Marseille, Marseille, France), Jason Glenn (University of Colorado, Boulder, CO), Professor Matthew Griffin (Cardiff University), Dr Peter Hargrave (Cardiff University) and Bruce Sibthorpe (Cardiff University).

The work covered in this paper was funded by the School of Graduate Studies at the University of Lethbridge (JVL), the Canadian Institute for Photonics Innovations (JVL), the Canadian Space Agency (DAN, JVL) and the National Science and Engineering Research Council (DAN, JVL).

REFERENCES

1. M. J. Griffin and B. M. Swinyard, "Herschel-SPIRE: design, performance, and scientific capabilities," in *Space Telescopes and Instrumentation I: Optical, Infrared, and Millimeter (this volume)*, **6265**, Proceedings of the International Society for Optical Engineering, 2006.
2. G. L. Pilbratt, "Herschel mission: status and observing opportunities," in *Space Telescopes and Instrumentation I: Optical, Infrared, and Millimeter (this volume)*, **6265**, Proceedings of the International Society for Optical Engineering, 2006.
3. B. M. Swinyard, K. Dohlen, M. Ferlet, J. Glenn, and J. J. Bock, "Optical performance characterization of Herschel/SPIRE," in *Space Telescopes and Instrumentation I: Optical, Infrared, and Millimeter (this volume)*, **6265**, Proceedings of the International Society for Optical Engineering, 2006.

4. T. L. Lim, B. M. Swinyard, A. A. Aramburu, J. J. Bock, M. J. Ferlet, T. R. Fulton, D. Griffin, M. J. Griffin, S. J. Leeks, D. A. Naylor, D. Rizzo, E. C. Sawyer, B. Schulz, S. D. Sidher, L. D. Spencer, D. L. Smith, T. J. Waskett, and A. L. Woodcraft, "Preliminary results from Herschel-SPIRE flight model testing," in *Space Telescopes and Instrumentation I: Optical, Infrared, and Millimeter (this volume)*, **6265**, Proceedings of the International Society for Optical Engineering, 2006.
5. J. V. Lindner, "SHIFTS: Simulator for the Herschel Imaging Fourier Transform Spectrometer," Master's thesis, University of Lethbridge, Lethbridge, AB, 2006.
6. B. Sibthorpe, A. Woodcraft, and M. Griffin, "A software simulator for the Herschel-SPIRE imaging photometer," in *Optical, Infrared, and Millimeter Space Telescopes*, J. C. Mather, ed., **5487**, pp. 491–500, Proceedings of the International Society for Optical Engineering, 2004.
7. B. M. Swinyard, K. Dohlen, D. Ferand, J.-P. Baluteau, D. Poulouen, P. Dargent, G. Michel, J. Martignac, P. Ade, P. Hargrave, M. Griffin, D. Jennins, and M. Caldwell, "The Imaging FTS for Herschel SPIRE," in *IR Space Telescopes and Instruments*, J. C. Mather, ed., **4850**, pp. 698–709, Proceedings of the International Society for Optical Engineering, 2003.
8. P. A. R. Ade, P. Hamilton, and D. A. Naylor, "An Absolute Dual Beam Emission Spectrometer," in *Fourier Transform Spectroscopy: New Methods and Applications*, pp. 90–92, Optical Society of America, (Santa Barbara, CA), 1999.
9. P. C. Hargrave, J. W. Beeman, P. A. Collins, I. Didschuns, M. J. Griffin, B. Kiernan, and G. Pisano, "In-Flight Calibration Sources for Herschel-SPIRE," in *IR Space Telescopes and Instruments*, J. C. Mather, ed., **4850**, pp. 638–649, Proceedings of the International Society for Optical Engineering, 2003.
10. S. P. Davis, M. C. Abrams, and J. W. Brault, *Fourier Transform Spectroscopy*, Academic Press, St. Louis, MO, 2001.
11. D. Griffin, M. Griffin, and B. Swinyard, "SPIRE Design Description," Tech. Rep. SPIRE-RAL-PRJ-000620, Rutherford Appleton Laboratory, Oxfordshire, England, 2003.
12. A. D. Turner, J. J. Bock, J. W. Beeman, J. Glenn, P. C. Hargrave, V. V. Hristov, H. T. Nguyen, F. Rahman, S. Sethuraman, and A. L. Woodcraft, "Silicon nitride micromesh bolometer array for submillimeter astrophysics," *Applied Optics* **40**(28), pp. 4921–31, 2001.
13. R. J. Hanisch, A. Farris, E. W. Greisen, W. D. Pence, B. M. Schlesinger, P. J. Teuben, R. W. Thompson, and A. Warnock, "Definition of the Flexible Image Transport System (FITS)," *Astronomy and Astrophysics* **376**(1), pp. 359–380, 2001.
14. D. A. Naylor, J.-P. Baluteau, P. Davis-Imhof, M. J. Ferlet, T. R. Fulton, and B. M. Swinyard, "Performance evaluation of the Herschel/SPIRE imaging Fourier transform spectrometer," in *Space Telescopes and Instrumentation I: Optical, Infrared, and Millimeter (this volume)*, **6265**, Proceedings of the International Society for Optical Engineering, 2006.
15. L. D. Spencer, D. A. Naylor, and B. M. Swinyard, "A comparison of the theoretical and measured instrumental line shape of the Herschel/SPIRE imaging Fourier transform spectrometer," in *Space Telescopes and Instrumentation I: Optical, Infrared, and Millimeter (this volume)*, **6265**, Proceedings of the International Society for Optical Engineering, 2006.
16. T. Fulton, "SPIRE Detector Response and Glitch Characterization," Tech. Rep. SPIRE-UOL-REP-002207, University of Lethbridge, Lethbridge, AB, 2005.
17. D. A. Naylor, T. R. Fulton, P. W. Davis, I. M. Chapman, B. G. Gom, L. D. Spencer, J. V. Lindner, N. E. Nelson-Fitzpatrick, and G. R. Davis, "Data processing pipeline for a time-sampled imaging Fourier transform spectrometer," in *Imaging Spectrometry X*, S. S. Shen and P. E. Lewis, eds., **5546**, pp. 61–72, Proceedings of the International Society for Optical Engineering, 2004.
18. M. Griffin, "SPIRE Sensitivity Models," Tech. Rep. SPIRE-QMW-NOT-000642, Cardiff University, Cardiff, Wales, 2004.